Available online at www.sciencedirect.com
SCIENCE DIRECT®
Energy and Buildings 37 (2005) 399–409
ENERGY and BUILDINGS
www.elsevier.com/locate/enbuild

A model for an under floor air distribution system

Y.J.P. Lin[a,*], P.F. Linden[b]

[a]*Energy and Resources Laboratories, Industrial Technology Research Institute, Hsinchu 310, Taiwan*
[b]*Department of Mechanical and Aerospace Engineering, University of California, 9500 Gilman Drive La Jolla, San Diego, CA 92093-0411, USA*

Received 15 April 2004; received in revised form 30 July 2004; accepted 31 July 2004

Abstract

We present a simplified model of an underfloor air distribution (UFAD) system consisting of a single source of heat and a single cooling diffuser in a ventilated space. Laboratory experiments were carried out to simulate the flow and a model for the flow in this space is proposed. The model is based on plume theory for the heat source and a fountain model for the diffuser flow, and predicts a steady-state two-layer stratification in the room. The governing parameters are shown to be the buoyancy flux of the heat source, and the volume and momentum fluxes of the cooling diffuser. The results suggest ways to optimize UFAD design and operation.

Keywords: UFAD system; Penetrative entrainment; Turbulent plume; Turbulent fountain; Displacement ventilation; Mixing ventilation

1. Introduction

The motivation for this study is to understand and model the behavior of an under floor air distribution system (hereafter referred to as UFAD) in a ventilated room. This system was first introduced in the 1950s to cool a computer room and is emerging as a leading ventilation system design in modern commercial buildings. According to Loudermilk [1], two major advantages of this system are:

- ventilation cool air is certain to reach the occupants (as it is introduced within the occupied zone);
- convection heat gains that occur above the occupied zone are isolated from the calculation of the required space supply air flow.

The displacement-type flow, that occurs in the upper zone, serves to convey heat efficiently to ceiling-based exhaust openings, resulting in better cooling efficiency and indoor air quality in the lower, occupied portion of the space, than those of the traditional mixing type systems.

Bauman and Webster [2] show that well-designed UFAD systems can provide such benefits as:

- reduced life cycle building costs;
- improved thermal comfort;
- improved ventilation efficiency and indoor air quality;
- reduced energy use;
- reduced floor-to-floor height in new constructions;
- improved productivity and health.

Despite these potential advantages of underfloor systems, barriers exist to widespread adoption of the UFAD technology. According to [2], there is a higher risk to designers and building owners due to a lack of objective information and standardized design guidelines. The aim of this research is to provide some guidelines for this new emerging cooling strategy.

Traditional over-head air-conditioned systems introduce conditioned cool air from above. This geometrical design induces entrainment of warm air at the top of the room into the conditioned air, so the temperature of the conditioned cool air when it arrives at the floor level is higher than the supply value (Fig. 1). This geometrical arrangement induces

* Corresponding author. Tel.: +886 3 591 6446; fax: 886 3 582 0250.
E-mail address: peteryjlin@itri.org.tw (Y.J.P. Lin).

0378-7788/$ – see front matter © 2004 Elsevier B.V. All rights reserved.
doi:10.1016/j.enbuild.2004.07.011

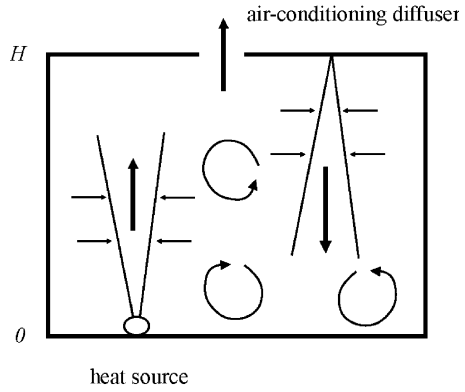

Fig. 1. A simple illustration of a traditional over-head cooling ventilation system in a ventilated room having one heat source and one cooling diffuser.

the flow pattern known as mixing ventilation in the space, so the vertical air temperature profile is almost uniform.

The UFAD system introduces the conditioned air at floor level (Fig. 2), which allows the temperature of the supply air to be the same as, or slightly lower than, the required comfort temperature for occupants in the room. Thus, the UFAD system is able to use a higher supply temperature and, therefore, consumes less energy than the traditional over-head system for the same cooling load. In addition to the advantage of energy conservation, with appropriate design geometry, an UFAD system induces an efficient ventilation pattern in a room, producing good indoor air quality and cooling efficiency.

In comparison with classic displacement ventilation systems that deliver air at low velocities at the bottom of the space, typical UFAD systems deliver air through floor diffusers with higher supply air velocities. In addition to increasing the amount of mixing (and therefore potentially diminishing the ventilation performance compared to

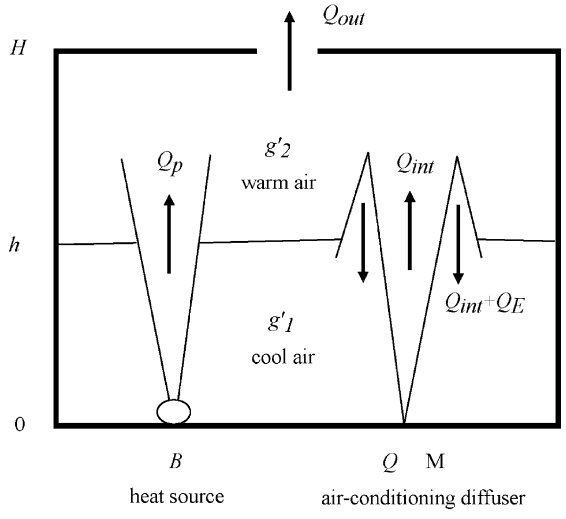

Fig. 2. A simple sketch of an UFAD system in a room having a ceiling exhaust opening with one heat source and one cooling diffuser inside the space.

displacement ventilation systems), these more powerful supply air conditions can have significant impacts on room air stratification and thermal comfort in the occupied zone.

When the conditioned cool air from the diffuser has enough vertical momentum, this air will penetrate into the warm upper region and bring warm air down into the lower region. The amount of air brought down determines the temperature in the lower region (Webster et al. [3]). In the limit, as the input momentum and the amount of mixing is reduced, UFAD systems tend to approach the operation of displacement ventilation systems.

Ito and Nakahara [4] developed a simplified model to calculate the vertical space air temperature distribution in a ventilated space with an UFAD system. Suggested by measurements of the air temperature profile and visualization of the airflow, they divided the space into two regions: a completely mixed layer at the lower part of the room and a piston-flow region, the region above the interface where the air is assumed to flow vertically at a constant uniform velocity, as an upper layer. The heat balance equations were derived from the assumption that the discharged cool air completely mixed with the room air in the lower layer, while the room air moved upward to the ceiling only in the upper layer.

Zhang [5] developed a similar model as that of [4], with two regions in a ventilated space. Three sub-models, a thermal plume model (Morton et al. [6]), a multiple-layer model (Linden and Cooper [7]) and a room heat transfer model (Mundt [8], Li et al. [9]), were integrated in the model. In order to understand details of the airflow pattern in the room, Zhang applied a thermal plume model and a multiple-layer model. He adopted a heat transfer model to take the radiation into account, in addition the convective heat transfer.

The vertical momentum of the cooling diffuser has a strong impact on the vertical stratification in the space. Models that neglect the effect of the vertical momentum on vertical air stratification are more appropriate for wall-mounted diffusers at floor level (Fig. 3(a)). Conditioned air is introduced horizontally into the space at the floor level and distributed homogeneously at the floor level in the space. This system will be described theoretically in terms of a simple displacement ventilation model in Section 2.1.

Skistad et al. [10] addressed the qualitative impacts of this vertical momentum from the supply diffusers on the air stratification profile (see Section 4.6 of their book). When using floor-mounted diffusers, which are used commonly in the UFAD systems, it is important to apply optimal properties of the supply airflow. The high momentum might bring too much air into the upper layer, so that mixing ventilation is created and ventilation efficiency is reduced. On the other hand, low momentum might provide supply air without sufficient mixing with the room air, which creates a cold air layer along the floor.

In this paper, we discuss the fluid mechanics of UFAD systems and present a quantitative study of the vertical stratification distribution. We restrict attention to the simplified case of a single cooling diffuser and a single

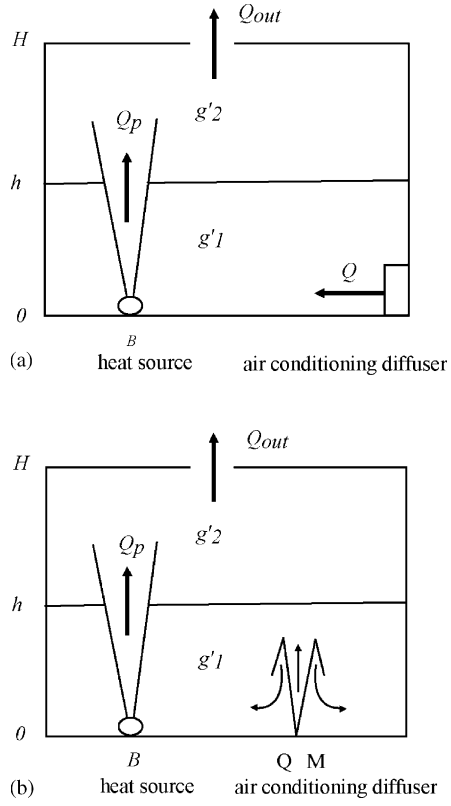

Fig. 3. Displacement ventilation occurs in a single room with a heat source and a cooling diffuser: (a) when the diffuser supply is horizontal, and (b) when the vertical momentum flux of the cooling diffuser too small to penetrate the density interface.

heat source at the same height in the room, with an extract at the ceiling, and examine the steady-state produced by them. A model based on plume theory for the heat source and a fountain model for the cooling diffuser, and based on a steady-state two-layer stratification is proposed. Fig. 2 shows a geometrical illustration of this simplified case.

The important parameters affecting the stratification and the performance of UFAD systems are discussed in Section 2, along with the theoretical model. The experiments, in Section 3, used a salt solution source as a plume source and a fresh water source as a fountain source in a water tank to simulate the airflow in the space equipped with UFAD systems. Section 4 presents our experimental observations qualitatively, and Section 5 presents comparisons of the experimental results with the theoretical predictions of the physical model. Numerical simulation, based on this model, of a full-scale room is presented in Section 6. The sensitivity of the performance of UFAD to the properties of the cooling diffuser and the heat source is discussed in Section 7. Finally, Section 8 gives the conclusions of this study.

2. Theoretical model

We consider the steady-state ventilation flow and the stratification in a room with a UFAD system consisting of one heat source and one cooling diffuser both located on the floor. The air in the space is extracted through a ceiling opening (Figs. 2 and 3). Warm air, which is produced by the heat source, rises to the ceiling and forms an upper layer of buoyant air. Conditioned cool air is supplied from the floor level by a cooling diffuser. The parameters governing the flow are the buoyancy flux B of the heat source, the volume flux Q and vertical momentum flux M of the cooling diffuser. However, different approaches and properties of supplying conditioned cool air result in different stratification profiles and ventilation patterns.

When the vertical momentum from the cooling diffuser is not significant, as shown in Fig. 3(a) and (b), so that supply cool air does not penetrate into the upper buoyant layer, pure displacement ventilation occurs. In this case, only the buoyancy flux B of the heat source and the volume flux Q from the diffuser are relevant parameters.

On the other hand, for sufficiently large vertical momentum flux M, the cool air from the diffuser interacts with the upper region. Then this ventilation pattern is a hybrid between mixing and pure displacement ventilation.

We assume that all the walls are adiabatic to the room environment. We also ignore any effects of heat conduction and radiation. Although a heat source and a cooling diffuser both located on the floor level of a ventilated room having a ceiling opening is considered here, the results apply equally to a cool source and a heating diffuser located on the ceiling of a ventilated room having a floor opening, provided temperature differences are small enough for the Boussinesq approximation to be valid.

2.1. Displacement ventilation model

We begin by discussing pure displacement ventilation. A two-layer stratification is established in the space because of density differences produced by the buoyancy sources. The upper layer is formed by the supply from the heat plume, and the lower layer by the supply from the cooling diffuser. Mass exchange between these two layers only occurs inside the plume at the density interface; elsewhere the interface separates the two different regions. The air in the upper layer exits through the ceiling opening at the rate Q given by the input volume flux from the diffuser. This volume flux is also equal to the volume flux Q_p in the plume at the height of the interface (see Fig. 3(a) and (b)).

This volume conservation is expressed as

$$Q = Q_p = Q_{out}, \tag{1}$$

where Q_{out} is the volume flux leaving the room.

The buoyancy force is conveniently described in terms of a reduced gravity

$$g' = \frac{\rho_r - \rho}{\rho_r} g, \tag{2}$$

where ρ is the density of air, ρ_r the reference density and g the gravitational acceleration. The Boussinesq approxima-

tion is applied in this analysis, so the density difference $\Delta\rho = \rho_r - \rho$ is assumed to be much smaller than the reference density ρ_r, i.e. $\Delta\rho \ll \rho_r$.

For air, well represented as an ideal gas, the reduced gravity is

$$g' = \frac{T - T_r}{T_r} g, \tag{3}$$

where T_r is the reference temperature and T the temperature of the air, and temperatures are in K. Thus, the Boussinesq approximation implies $T - T_r \ll T_r$; since typically $T - T_r \approx 5$ K and $T_r \approx 300$ K, this approximation is easily satisfied.

Here we choose the density of the air from the cooling diffuser ρ_f as the reference density ρ_r. Since there is no mixing, the reduced gravity in the bottom layer g'_1 (which corresponds to the temperature T_1) is the same as that from the cooling diffuser g'_f (or T_f), i.e.

$$g'_1 = g'_f = 0. \tag{4}$$

When the steady two-layer stratification is established, the density of the upper buoyant layer is the same as that of the plume at the density interface. For a self-similar plume (see [6]), the equations of the volume flux Q_p in the plume and the mean reduced gravity g'_p are given in terms of the buoyancy flux B of the plume source and the distance z from the plume source as

$$B = g'_p Q_p = \text{constant}, \tag{5a}$$

$$Q_p = Q_p(B, z) = C(Bz^5)^{1/3} \tag{5b}$$

and

$$g'_p = g'_p(B, z) = \frac{1}{C}(B^2 z^{-5})^{1/3}, \tag{5c}$$

where $C = (6/5)\alpha((9/10)\alpha)^{1/3}\pi^{2/3}$ and α is the entrainment constant for a buoyant plume.

Therefore, the volume flux in the plume at the interface is

$$Q_p(B, h) = CB^{1/3}h^{5/3}, \tag{6}$$

which is equal to the volume flux Q from the cooling diffuser and the volume flux Q_{out} leaving the space, as shown in Eq. (1). The reduced gravity g'_2 of air in the upper layer is determined by the buoyancy flux B of the heat source and the vertical distance h from the interface height to the origin of the plume, i.e.

$$g'_2 = g'_p(B, h) = \frac{1}{C}B^{2/3}h^{-5/3}. \tag{7}$$

The reduced gravity g'_2 of the upper layer of the steady-state is also determined by the buoyancy conservation equation, i.e.

$$g'_2 = \frac{B}{Q_{out}}, \tag{8}$$

since the buoyancy flux $g'_2 Q_{out}$ leaving the space is equal to the input buoyancy flux B.

Therefore, in this displacement model, once the supply volume flux Q is given with a fixed heat source B, the quantitative values of other parameters in the space can be solved analytically. Eqs. (6) and (8) can be rewritten as

$$h = \frac{Q^{3/5}}{C^{3/5}B^{1/5}} \tag{9}$$

and

$$g'_2 = \frac{B}{Q}. \tag{10}$$

When the heat source is fixed, the interface height h is proportional to the 3/5 power of the volume flux from the cooling diffuser. Increasing the ventilation flow rate raises the interface height by Eq. (9) and reduces the temperature of the upper layer according to Eq. (10).

2.2. UFAD ventilation model

When the vertical momentum flux M from the cooling diffusers is sufficient to penetrate the density interface, the consequence of mixing with the upper layer needs be taken into account. Cool air forced upwards by the momentum of the input crosses the interface into the upper layer. The cool air then falls back towards the floor entraining some of the warm air from the upper layer during its penetration through the density interface. The configuration is depicted schematically in Fig. 2.

We assume, in a steady-state, that a two-layer stratification forms as in Section 2.1, and this assumption is confirmed by experimental observations (see Section 4). Volume conservation in the space is again given by

$$Q = Q_{out}. \tag{11}$$

When the vertical momentum of a turbulent fountain is large enough to cause penetrative entrainment of upper layer fluid into the lower layer, the volume flux supplied to the upper layer by the plume increases, with volume flux Q_E, to include this entrained volume flux. In this case, volume flux conservation in the upper layer is now modified from Eq. (1) to

$$Q_p = Q_{out} + Q_E. \tag{12}$$

As before, buoyancy conservation in the room is

$$g'_2 Q_{out} = B, \tag{13}$$

so the upper layer temperature is the same as for displacement ventilation. Since the penetrative entrainment by the turbulent cool fountain brings some hot buoyant air into the lower layer, the reduced gravity of the lower layer is no longer equal to that from the fountain source, but has a value between that of the upper layer and that from the fountain source, i.e. $g'_f < g'_1 < g'_2$.

The volume flux Q_p in the plume at the density interface is again given by

$$Q_p(B,h) = C(Bh^5)^{1/3}, \tag{14a}$$

and the reduced gravity step across the interface is

$$\Delta g'(B,h) = g'_2 - g'_1 = \frac{1}{C}(B^2h^{-5})^{1/3}. \tag{14b}$$

Eqs. (11) and (13) can be rewritten as

$$g'_2 = \frac{B}{Q}, \tag{15}$$

which is the same as that for the displacement case (see Eq. (10)), and from Eqs. (12) and (14a) we have

$$h = \frac{(Q+Q_E)^{3/5}}{C^{3/5}B^{1/5}}. \tag{16}$$

Comparison of Eq. (16) for UFAD ventilation with Eq. (9) for displacement ventilation, having the same heat flux B and volume flux Q, shows that the interface height h increases as a result of penetrative entrainment by the diffuser. This entrainment increases the volume flux carried by the plume through the interface $Q + Q_E > Q$.

In contrast to displacement ventilation where the lower layer is at the supply temperature, the temperature of the lower layer in UFAD ventilation depends on the mixing of warm air from the upper part of the room. Therefore, one more equation is needed to solve the problem. We assume that the volume flux entrained by the fountain across the interface is proportional to the volume flux Q_{int} in the fountain at the interface. Thus

$$Q_E = EQ_{int}, \tag{17}$$

where E is a penetrative entrainment constant.

Using Eq. (17) and balancing the buoyancy inputs and outputs for the lower layer, we find the reduced gravity g'_1 of the lower layer is given by

$$g'_1 = \frac{g'_2Q_E + g'_fQ + g'_1(Q_{int} - Q)}{Q_E + Q + (Q_{int} - Q)}. \tag{18a}$$

The fluid entrained into the fountain in the lower layer has the volume flux $Q_{int} - Q$ and reduced gravity g'_1, and this fluid falls back to the lower layer. That does not change the stratification in the space. This fluid enters the upper layer and circulates back to the lower layer. However, this fluid entrains upper layer fluid into the lower layer and provides an additional heat flux g'_2Q_E into the lower layer. Therefore, the lower layer buoyancy is also expressed as

$$g'_1 = \frac{g'_2Q_E + g'_fQ}{Q_E + Q}. \tag{18b}$$

Since ρ_f is used as the reference density here, $g'_f = 0$. Hence (18a) and (18b) are also expressed as

$$g'_1 = \frac{g'_2Q_E}{Q_E + Q}. \tag{18c}$$

Eq. (18c) is consistent with Eq. (4) in the displacement ventilation when there is no penetrative entrainment at the interface, $Q_E = 0$ and $g'_1 = 0 = g'_f$. When the vertical diffuser momentum increases, the penetrative entrained volume flux Q_E increases. The reduced gravity g'_1 in the lower layer approaches the reduced gravity g'_2 in the upper layer as the vertical momentum flux increases. In the limit of large momentum flux, $Q_E \gg Q$, the whole space becomes well mixed (and $g'_1 \approx g'_2$).

A study of penetrative entrainment at the interface due to a fountain is addressed in Lin and Linden [11] (see also Chapter 4 of Lin [12]). The penetrative entrainment constant E was measured in separate experiments and was found to be $E = 0.6 \pm 0.1$. We estimate Q_{int} by the fountain model of Bloomfield and Kerr [13], solved via an explicit Euler numerical scheme.

Note that the effects of boundaries are not taken into account in the quantitative estimation of the penetrative entrained volume fluxes. If the diffuser jet hits a boundary, such as a sidewall or, more importantly, the ceiling, the penetrative entrainment rate will be changed from the free case. However, the equations in this section are still valid except Eq. (17). It would be necessary to re-evaluate the penetrative entrainment rate E in these cases.

3. Experiments

Experiments were conducted in two different Plexiglas water tanks using salt solutions to simulate airflow inside buildings (Linden et al. [14], and Baker and Linden [15]). The first has width $W = 15.0$ cm, height $H = 30.0$ cm and length $L = 30.0$ cm, and is filled to a depth of 23.0 cm with fresh water at the beginning of the experiment; this tank is denoted as Tank 1. The second has $W = 28.0$ cm, $H = 58.5$ cm and $L = 58.5$ cm, and is filled with water to 25.0 cm; this tank is denoted as Tank 2. Two sources were placed in the tank: a salt solution plume source simulating a heat source and a fresh water jet source simulating a cooling diffuser. Both sources were located at the level of the water surface. A siphon pipe, with inlet at the tank base, was connected to a constant head drain to keep a constant volume in the tank during the experiment. The geometry of this arrangement is inverted from a real UFAD system. In the following, the description and the results are presented as though the experiment is inverted (see Fig. 4(a)) so that they correspond to the ventilation orientation.

From our experimental observations, we find that a steady-state was reached after the fresh water jet injects 8–10 times as much fluid as the tank volume to replace the fluid in the tank. The smaller size of Tank 1 reduces the time to

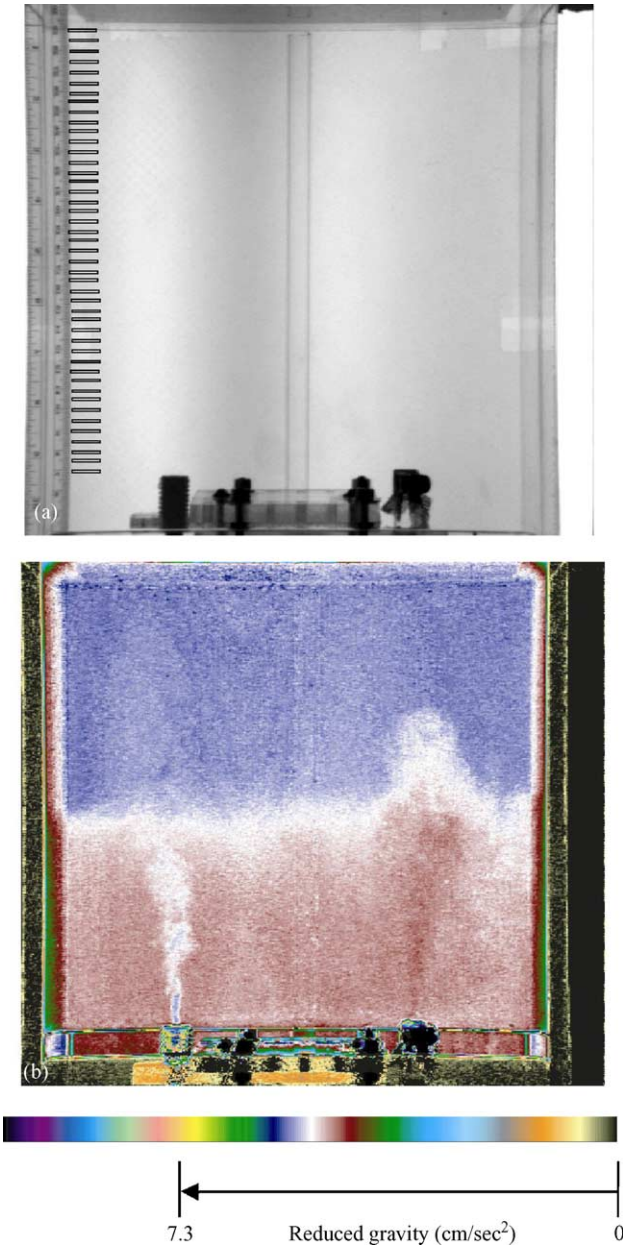

Fig. 4. The orientation of this experimental arrangement is inverted to be consistent with the UFAD system. (a) An image before running an experiment, and positions of the windows for measuring the light intensity in the tank. (b) An image of light intensity of Run 2 in the steady-state after correction for variations in the background lighting. The intensity scale for this experiment is corresponding to the reduced gravity from 0 to 7.3 cm/s^2.

attain the steady-state significantly compared to the larger one (Tank 2).

The plume nozzle is the same as the one used in Lin and Linden [16]. It is 0.5 cm in diameter, and the detail of the plume nozzle design is described in Hunt and Linden [17]. There are two different fountain nozzles used in the experiments; in Tank 1 a fountain nozzle was 1.27 cm in diameter, and in Tank 2 a fountain nozzle was 0.5 cm in diameter. Each of their exits was covered with wire mesh to promote disturbance of the flow and generate a turbulent jet.

The optical technique developed by Cenedese and Dalziel [18] was used to measure the density in the tank. Dye was added to the plume source and acted as a tracer for density. The intensity attenuation due to the dye under a constant light source was used to determine the local density averaged across the width of the tank. Fig. 4(b) shows an image of light intensity after correction for the background lighting. The positions of the windows for measuring the light intensity in the tanks are shown in Fig. 4(a). Each two adjacent windows have an interval of 0.5 cm between them. The window size in Tank 1 is 2 pixels high by 30 pixels wide (about 0.1 cm high by 2.0 cm wide in real scale), and that in Tank 2 is 2 pixels high by 38 pixels wide (about 0.2 cm high by 5.5 cm wide in real scale).

When a fixed cross-section area nozzle is used, the momentum flux varies with the volume flux. The momentum flux M is related to the cross-section area A and the volume flux Q of the nozzle by

$$M = \frac{4}{3}\frac{Q^2}{A}, \tag{19}$$

assuming that the exit flow has a parabolic-shape velocity profile. This is a reasonable assumption for the velocity profile at the exit of the pipe flow. Therefore, two different nozzles were used to produce different initial volume fluxes at almost the same momentum flux (Runs 2 and 3 in Table 1), or different initial momentum fluxes at almost the same volume flux (Runs 2 and 4), in order to isolate the effects of variations in M and Q.

4. Qualitative observations

The plume and fountain sources were both positioned at the floor level ($z = 0$) in all cases. When the fountain nozzle and the plume nozzle were turned on, the fluid from the plume source entrained the ambient fluid as it ascended, spread out at the ceiling of the tank and pushed down ambient fluid, thereby establishing an upper layer. The fountain source injects fluid upwards, which penetrates some distance into the upper layer and brings some of the upper layer fluid to the lower layer. The two-layer structure, the plume and the flow from the diffuser penetrating into the upper layer can be seen in Fig. 4(b).

The time to reach a steady-state depends on the size of the tank and the volume flux of the fountain source that replaces the fluid in the tank. The lower layer is supplied by the fluid

Table 1
The experimental conditions of four different runs (D is the diameter of fountain nozzle exit)

Run no.	B (cm^4/s^3)	M (cm^4/s^2)	Q (cm^3/s)	D (cm)	Tank
1	63.2	228.1	17.0	1.27	1
2	63.2	150.3	13.8	1.27	1
3	59.1	154.1	5.5	0.5	2
4	59.5	770.5	12.3	0.5	2

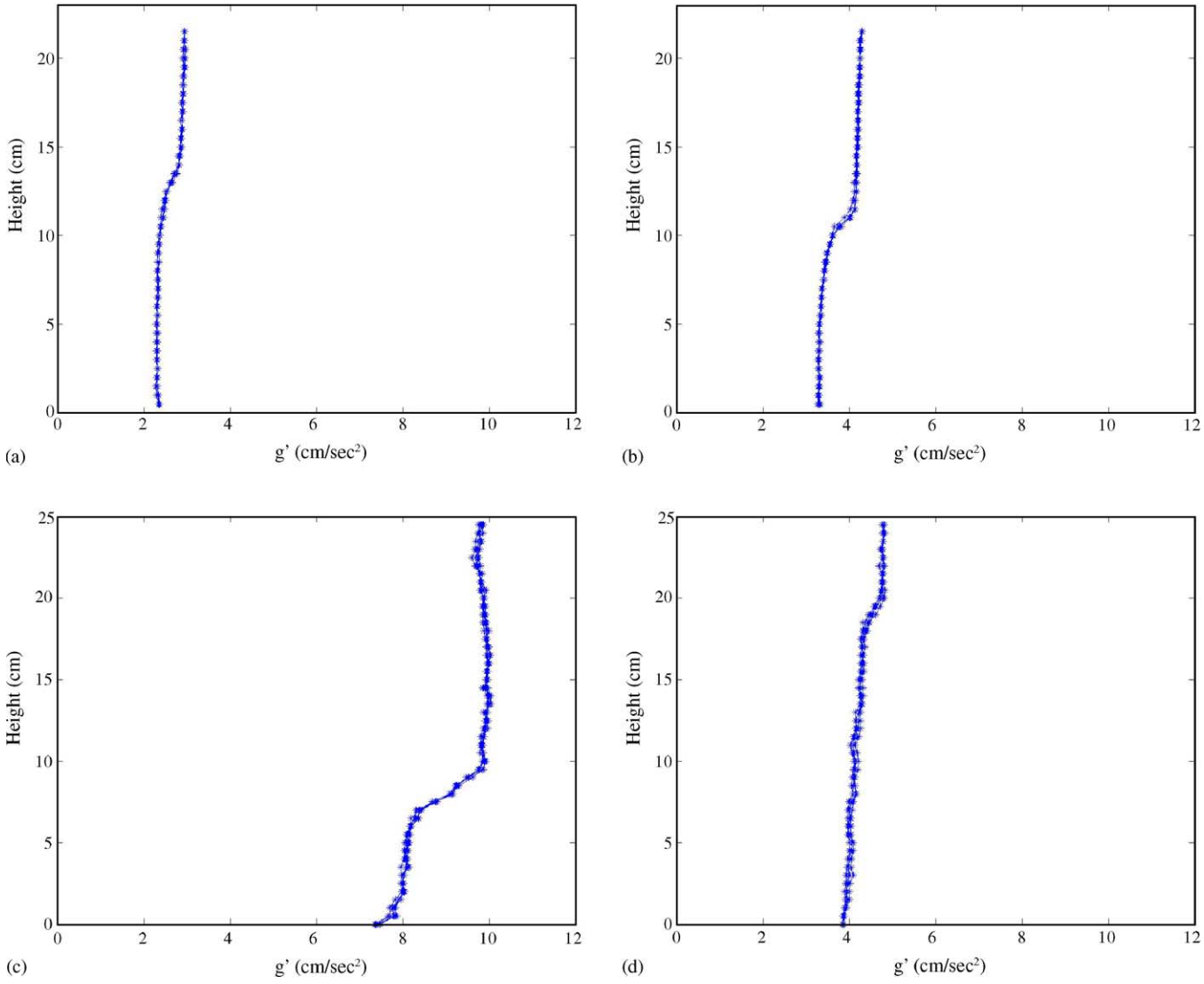

Fig. 5. The buoyancy profiles of (a), (b), (c), and (d) were measured in Runs 1, 2, 3 and 4, respectively. Each profile has five consecutive measurements with an interval of 1 min between each.

from the fountain and that entrained from the upper layer, and the fluid in this layer is taken out by lateral entrainment of the plume as it ascends. The supply volume flux and the size of the lower layer determine the time for the lower layer to reach a steady-state. The properties of the upper layer are determined by the fluid from the plume and the fluid of the lower layer, because the fluid from the plume source entrains the fluid of the lower layer, and supplies to the upper layer. The fluid in the upper layer is extracted by penetrative entrainment of the fountain, and the outflow.

The ventilation directions in the room, outside the plume and the fountain, are both downward in both layers. The fluid of the upper layer is supplied by the plume from below, and extracted at the opening of the ceiling and the penetrative entrainment at the interface. The fluid in the plume spreads out at the ceiling level and has a volume flux larger than the volume flux exiting the room, so the remaining fluid moves downwards. The fluid of the lower layer is extracted by lateral entrainment into the plume, and supplied by the fountain and its entrainment volume flux from the upper layer. This fluid comes from above, so the movement of the fluid in the lower layer is downward too.

We observed steady two-layer stratification in all the experimental cases. Fig. 5 shows vertical buoyancy profiles of the four experiments. Each profile in Fig. 5 has five consecutive measurements with an interval of 1-min between each. These measurements all superimpose together as one thick line, showing that a steady-state is achieved.

We maintained almost the same input buoyancy flux B in all the experiments (see Table 1). For the maximum Q, Run 1, we observe the smallest values of buoyancy (temperature) (Fig. 5(a)). When Q is decreased, so is M, and in Run 2, we observe the increasing values of buoyancy and the

decreasing interface height in the space (Fig. 5(b)), compared with Run 1. When the almost same M as Run 2 is produced and Q is decreased to the minimum value of all the experiments, in Run 3, we observe the interface is relatively close to the floor and the buoyancy in the space is large (Fig. 5(c)). Keeping a similar Q to Run 2 and increasing M significantly, in Run 4, we observe a similar magnitude of buoyancy and a much larger interface height, compared with Run 2 (Fig. 5(d)).

5. Comparisons with the model

Predictions of the theoretical model in Section 2.2 are compared with the experimental results in Section 5.1. Analyzed cases were confined to a certain range of momentum fluxes and volume fluxes such that the fountain did not reach the ceiling. We observed that, when $M \geq 530\ \mathrm{cm}^4/\mathrm{s}^2$, the fluid from the fountain source hit the ceiling of the tank. This boundary effect is a complex issue and beyond the scope of the theoretical model discussed in this paper, but some results for this case are discussed briefly in Section 5.2.

5.1. Without impingement on the ceiling

We apply a virtual origin correction for the plume (Hunt and Kaye [19]) in the calculations. The virtual origin length z_v for the plume in these experiments is from 1.03 to 1.1 cm. Then Eqs. (14a) and (14b) for this system become

$$Q_p(B_r, h) = C(B_r(h + z_v)^5)^{1/3}, \tag{20}$$

and

$$\Delta g'(B_r, h) = \frac{1}{C}(B_r^2(h + z_v)^{-5})^{1/3}. \tag{21}$$

In the lower layer, the buoyancy flux of the plume now becomes $B_r = (g'_s - g'_1)\, Q_s$, where g'_s and Q_s are the reduced gravity and volume flux of the plume source, respectively.

Buoyancy conservation of Eq. (13) gives the value of the upper layer reduced gravity g'_2. To improve the calculation accuracy of g'_2, the small volume flux Q_s (0.7 ml/s in all experiments and $Q_s \ll Q$ (see Table 1)) from the plume source is taken into account. Hence g'_2 is estimated by

$$g'_{2c} = \frac{B}{Q + Q_s}. \tag{22}$$

Fig. 6 shows the estimated values (g'_{1c}, g'_{2c} and h_c), using a minimum penetrative entrainment rate $E = 0.5$ and a maximum one $E = 0.7$, along with the experimental results.

Experiments of Runs 1 and 2 were conducted in Tank 1, with a large fountain source nozzle ($D = 1.27$ cm). Fig. 6(a) presents the theoretical predictions and the experimental results of Run 1. The predicted values of interface height $h_c = 14.3$ and 17.8 cm somewhat overestimate the experimental value $h_e = 14.1$ cm. The predicted values of the lower layer reduced gravity $g'_{1c} = 2.2$ and $2.5\ \mathrm{cm/s}^2$ span the experimental measured value $g'_{1e} = 2.3\ \mathrm{cm/s}^2$. The predicted value of the upper layer $g'_{2c} = 3.1\ \mathrm{cm/s}^2$ has a deviation $0.2\ \mathrm{cm/s}^2$ from the experimental value $g'_{2e} = 2.9\ \mathrm{cm/s}^2$. The light intensity technique is considered to have 10% deviations with the real buoyancy value. The difference between g'_{2c} and g'_{2e} is within the region of experimental uncertainty $\pm 0.1 g'_{2e}$.

Fig. 6(b) shows the theoretical predictions and the experimental results of Run 2. The predicted values of interface height $h_c = 11.3$ and 12.0 cm are in good agreement with the experimental value $h_e = 11.8$ cm. The predicted values of the lower layer reduced gravity $g'_{1c} = 2.9$ and $3.3\ \mathrm{cm/s}^2$ slightly underestimate the experimental measured value $g'_{1e} = 3.3\ \mathrm{cm/s}^2$. We present the results having the accuracy to $10^{-1}\ \mathrm{cm/s}^2$. Although the second prediction is the same as the experimental measurement, from Fig. 6(b) we can see the prediction is slightly below the experimental measurement. The difference between these two values is within $10^{-1}\ \mathrm{cm/s}^2$. The estimated value of the upper layer buoyancy $g'_{2c} = 4.4\ \mathrm{cm/s}^2$ has a difference of about $0.2\ \mathrm{cm/s}^2$ from the experimental value $g'_{2e} = 4.2\ \mathrm{cm/s}^2$.

Theoretical predictions of Run 3 have good agreement with the experimental results (Fig. 6(c)). The predicted values of the interface position ($h_c = 8.3$ and 13.7 cm) and the lower layer reduced gravity ($g'_{1c} = 7.4$ and $8.4\ \mathrm{cm/s}^2$) both span the experimental results ($h_e = 9$ cm and $g'_{1e} = 8.0\ \mathrm{cm/s}^2$). The estimated upper layer buoyancy $g'_{2c} = 9.5\ \mathrm{cm/s}^2$, by Eq. (22), has a difference of about $0.3\ \mathrm{cm/s}^2$ from the experimentally determined average buoyancy $g'_{2e} = 9.8\ \mathrm{cm/s}^2$. These differences are within the experimental uncertainty.

These results show that, when the fountain does not interact with the boundary, the UFAD model provides reasonable predictions with experimental results in the steady state. The theoretical predicted values are within 10% of the experimental results.

5.2. With impingement on the ceiling

When a turbulent fountain hits the ceiling, Eq. (17) is no longer valid. The penetrative entrainment assumption is based on a certain ratio of the available kinetic energy at the density interface being converted into the gained potential energy in the system. Since the boundary impact dissipates part of available kinetic energy, we expect the value E of the penetrative entrainment rate to be reduced.

In Run 4, the turbulent fountain had sufficient momentum to impinge on the ceiling of the tank. The upper layer buoyancy can still be estimated by Eq. (22), and we have $g'_{2c} = 4.6\ \mathrm{cm/s}^2$, in good agreement with the experimental measurement $g'_{2e} = 4.8\ \mathrm{cm/s}^2$ (see Fig. 5(d)). But the penetrative entrained volume flux by the turbulent fountain across a density interface is more complicated than that discussed in this paper. The model uses the minimum and maximum limits of penetrative entrainment rate $E = 0.5$ and

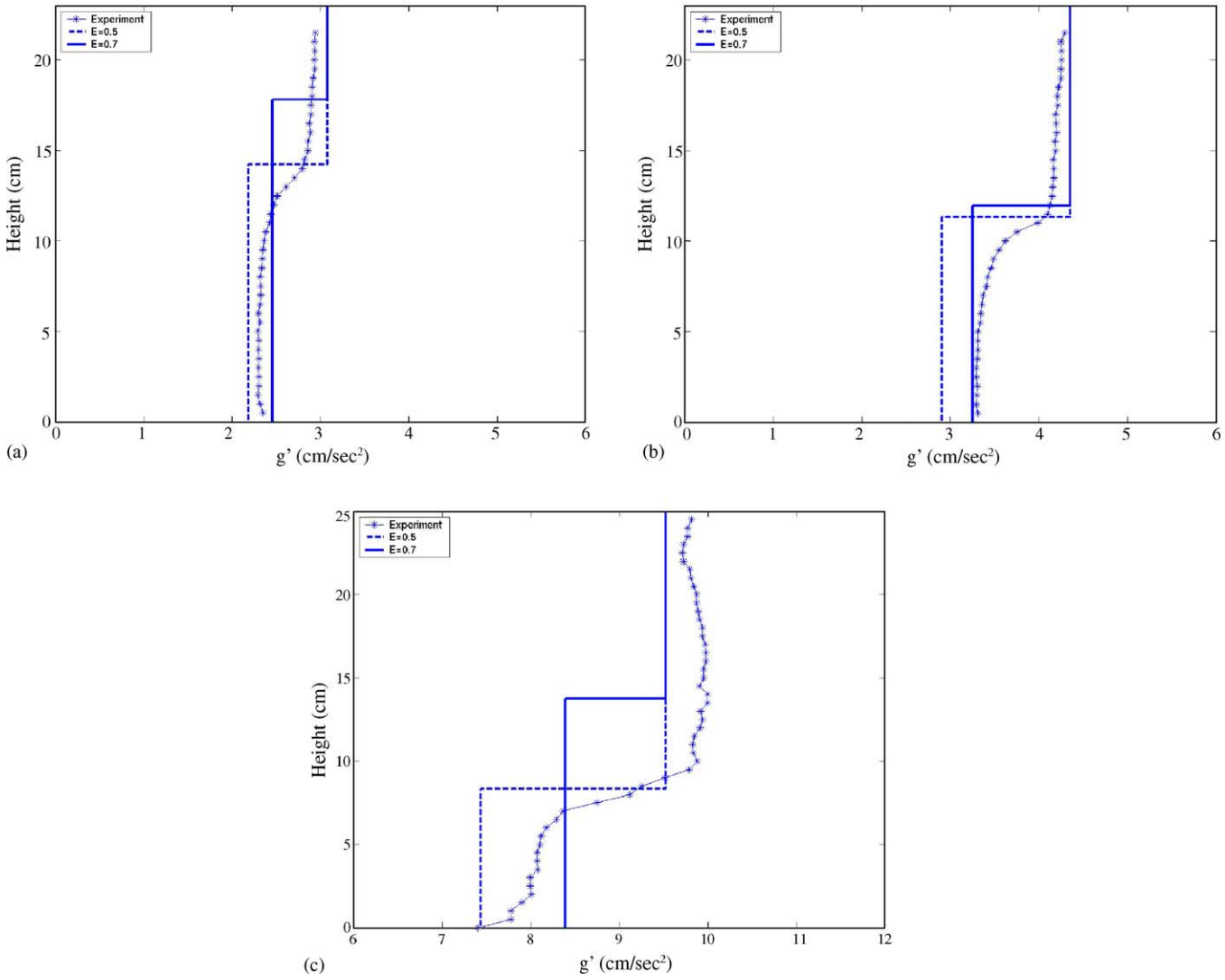

Fig. 6. The theoretical estimations are compared with the experimental results of (a) Run 1, (b) Run 2 and (c) Run 3.

0.7 to estimate the values of the interface height h_c, between 23.6 and 34.7 cm, and the lower layer buoyancy g'_{1c}, between 4.3 and 4.4 cm/s^2. The predicted interface position is significantly different from the experimental measurement $h_e = 19.5$ cm. However, the average measured value of the lower layer reduced gravity $g'_{1e} = 4.1$ cm/s^2 is not too far from the predicted values g'_{1c} although this model is not valid.

6. Numerical simulation

Eqs. (12), (14a), (14b) and (17) coupled with the fountain model of [13] are solved numerically to estimate the values of the lower layer reduced gravity g'_1 and the interface height h. Here we examine the effects of varying one of parameters B, Q or M. Typical parameters in the present design of UFAD systems (see [10]) are used in our stimulation. The room has a height of 3 m and a square area, with 4.8 m at each side. Supply air temperature (SAT) from the cooling diffuser is 20 °C.

Fig. 7(a) shows a case has the fixed input volume flux $Q = 6.6 \times 10^4$ cm^3/s (about 147 CFM) and momentum flux $M = 3.46 \times 10^6$ cm^4/s^2, and the heat flux H varies from 420 to 620 W. Linden [20] shows that flows driven by sources of heat with heat flux H are characterized by the buoyancy flux

$$B = \frac{g\gamma H}{\rho c_p}, \tag{23}$$

where γ is the coefficient of thermal expansion and c_p the specific heat capacity at constant pressure. Fig. 7(b) has the fixed heat flux $H = 520$ W and momentum flux $M = 3.46 \times 10^6$ cm^4/s^2, and Q is varied from 4.8×10^4 to 8.4×10^4 cm^3/s (about 107–187 CFM). Fig. 7(c) has the fixed heat flux $H = 520$ W and ventilation rate $Q = 6.6 \times 10^4$ cm^3/s, and M is varied from 2.46×10^6 to 4.46×10^6 cm^4/s^2.

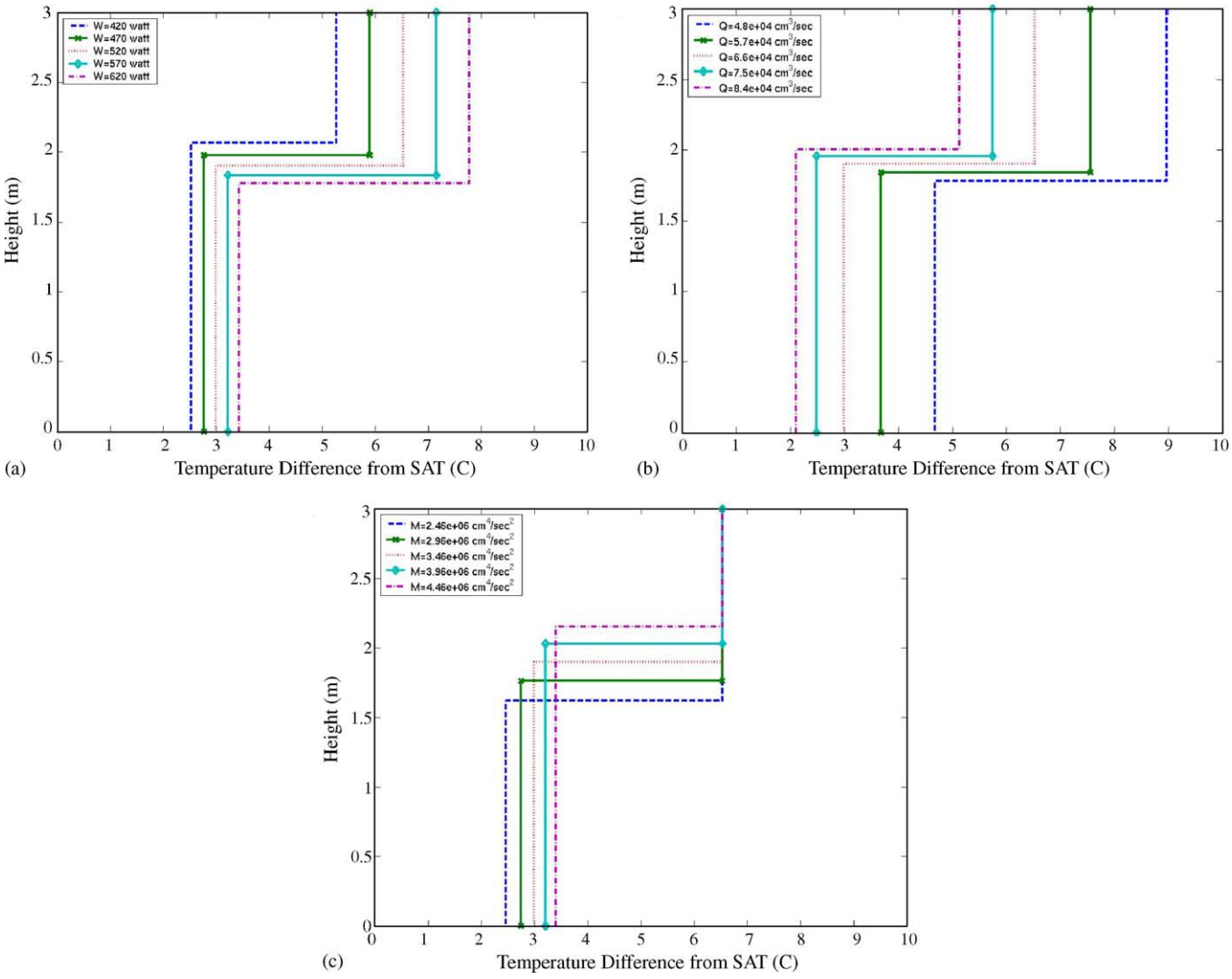

Fig. 7. Numerical simulation of the vertical stratified profiles in the space has (a) different heat loads, (b) different ventilation rates, and (c) different momentum fluxes when the other conditions are fixed.

The results of the model show predicted interface heights about 1.5–2 m. These show that for the typical conditions the cooled zone reaches up to about head height, as expected. The variations of interface height are quite modest for the parameter ranges under consideration. On the other hand, the lower zone temperature shows a significant variation (about 3 °C) with ventilation rate (Fig. 7(b)).

We can see the influence of a single parameter of B, Q or M on the flow stratification from the results of numerical simulations. When the heat load increases, the temperatures in the space (both layers) increase and the interface height reduces as shown in Fig. 7(a). When the ventilation flow rate increases, the height of the interface increases and the temperatures of the both layers decrease (see Fig. 7(b)). When the momentum flux increases, the interface height increases and the temperature contrast across the interface decreases (see Fig. 7(c)). The temperature contrast between two layers is related to the penetrative entrained volume flux by the fountain. The larger penetrative entrained volume flux results in a smaller temperature difference across two layers when the other conditions are fixed (see Eq. (18)).

7. Discussion

When the vertical momentum flux from the diffuser is small, the penetrative entrainment mechanism at the interface is not significant and a displacement model is suitable for design. As the vertical momentum flux increases, penetrative entrainment becomes important. In that case, the interface is raised above the height obtained by the displacement case and the lower layer temperature increases. A trade-off between these changes is required to obtain optimal performance from the UFAD system.

A two-layer stratification forms in the space when the steady state is reached. The interface height is controlled by

the ventilation rate and the momentum flux, while the temperature contrast between the two layers is set by the momentum flux. The heat load determines the temperature in the space for a given ventilation condition.

When the flow from the diffuser hits the ceiling, the theoretical model is still able to estimate the upper layer temperature but fails to estimate the interface height and the lower layer temperature. However, this case is of little practical importance, since the system is designed to have the cooling jets that terminate before they reach the ceiling.

8. Conclusions

We present a study of the steady-state flow driven by a heat source and an UFAD cooling diffuser in a ventilated space having a ceiling return. We have developed a new UFAD ventilation model for the flow in this specific space, and carried out laboratory experiments using the salt-bath technique to simulate the flow. Our study shows that the control parameters on the flow pattern are the buoyancy flux of the heat source, the volume flux and the momentum flux of the cooling diffuser.

Both qualitative behaviors and quantitative predictions of this system are presented. The UFAD ventilation model is applied to describe and estimate the properties of the indoor environment. The model explains plainly the qualitative observations from our experiments. Theoretical predictions by this model are in reasonable agreement with our experimental results.

Comparisons between the results of this research and the measurements of full-scale buildings are being conducted in order to provide some guidelines to building designers for designing UFAD systems.

Acknowledgments

The authors are grateful to Professor Colm Caulfield for his instructional suggestions on the experimental setup of this study. The first author wishes to thank Ministry of Education in Taiwan providing the scholarship for part of this work. The research is also supported by a grant from California Energy Commission.

References

[1] K.J. Loudermilk, Underfloor air distribution solutions for open office applications, ASHRAE Transactions 105 (1999) 605–613.
[2] F. Bauman, T. Webster, Outlook for underfloor air distribution, ASHRAE Journal 43 (6) (2001) 18–27.
[3] T. Webster, F. Bauman, J. Reese, Underfloor air distribution: thermal stratification, ASHRAE Journal 44 (5) (2002) 28–36.
[4] H. Ito, N. Nakahara, Simplified calculation model of room air temperature profile in under-floor air-condition system, in: International Symposium on Room Convection and Ventilation Effectiveness. ISRACVE, ASHRAE, 1993.
[5] Q. Zhang, Room Air Stratification Model for Underfloor Air Distribution System, Master thesis, University of Berkeley, 2000, 104 pp.
[6] B.R. Morton, G.I. Taylor, J.S. Turner, Turbulent gravitational convection from maintained and instantaneous sources, in: Proceedings of the Royal Society of London, A 234 (1196), 1956, pp. 1–23.
[7] P.F. Linden, P. Cooper, Multiple sources of buoyancy in a naturally ventilated enclosure, Journal of Fluid Mechanics 311 (1996) 177–192.
[8] E. Mundt, Convective flows above common heat sources in rooms with displacement ventilation, in: Proceeding of International Conference on Engineering Aero and Thermodynamics of Ventilated Room, ROOMVENT'90, Oslo, 1990.
[9] Y. Li, M. Sandberg, L. Fuchs, Vertical temperature profiles in rooms ventilated by displacement: full-scale measurement and nodal modeling, Indoor Air 2 (1992) 225–243.
[10] H. Skistad, E. Mundt, P. Nielsen, K. Hagstrom, J. Railio, Displacement Ventilation in Non-industrial Premises, Federation of European Heating and Air-conditioning Associations, ISBN 82-594-2369-3, 2002.
[11] Y.J.P. Lin, P.F. Linden, Penetrative entrainment of a turbulent fountain, Journal of Fluid Mechanics, 2004, submitted for publication.
[12] Y.J.P. Lin, Plumes and jets in semi-confined space, Ph.D. thesis, University of California, San Diego, 2003, 181 pp.
[13] L.J. Bloomfield, R.C. Kerr, A theoretical model of a turbulent fountain, Journal of Fluid Mechanics 424 (2000) 197–216.
[14] P.F. Linden, G.F. Lane-Serff, D.A. Smeed, Emptying filling boxes: the fluid mechanics of natural ventilation, Journal of Fluid Mechanics 212 (1990) 300–335.
[15] N. Baker, P.F. Linden, Physical modeling of airflows—a new design tool, in: F. Mills (Ed.), Atrium Build Archit. Eng., CICC Publications, Welwyn, England, 1991, pp. 13–22.
[16] Y.J.P. Lin, P.F. Linden, Buoyancy-driven ventilation between two chambers, Journal of Fluid Mechanics 463 (2002) 293–312.
[17] G.R. Hunt, P.F. Linden, Steady-state flows in an enclosure ventilated by buoyancy forces assisted by wind, Journal of Fluid Mechanics 426 (2001) 355–386.
[18] C. Cenedese, S.B. Dalziel, Concentration and depth fields determined by the light transmitted through a dyed solution, in: Proceedings of the Eighth International Symposium on Flow Visualization, in: G.M. Carlomagno, L. Grant (Eds.), ISBN 0953399109, paper 061, 1998.
[19] G.R. Hunt, N.G. Kaye, Virtual origin correction for lazy turbulent plume, Journal of Fluid Mechanics 435 (2001) 377–396.
[20] P.F. Linden, The fluid mechanics of natural ventilation, Annual Review of Fluid Mechanics 31 (1999) 201–238.